DOI: 10.1002/chem.200501159

Tuning of Electronic Properties in Thienyl-Phosphole π-Conjugated Systems through P-Functionalization Monitored by Raman Spectroscopy

Juan Casado,[a] Régis Réau,[b] and Juan T. López Navarrete*[a]

Abstract: Herein, a Raman spectroscopic study of a new family of 2,5-di(2-thienyl)phospholes and thienyl-capped 1,1′-diphospholes is presented. The Raman spectra have been carefully assigned with the help of density functional calculations. For di(2-thienyl)phospholes, two well-differentiated groups of Raman bands exist that arise either from the central phosphole ring or from the outer thiophene substituents. These data reveal a segmentation of the electronic structure. This paper reports interesting relationships between geometrical data such as the BLA (bond-length alternation) parameter and Raman band wavenumbers. These correlations are unprecedented in the chemistry of phospholes and have been used to interpret the evolution of the electronic structure (aromaticity⇄π-conjugation) upon 1) substitution of the central sulfur atom of terthiophene by phosphorus and 2) P-functionalization. Increasing the coordination number of the phosphole ring results in intramolecular charge transfer. The best scenario for phosphole aromaticity is found for 1,1′-diphospholes.

Keywords: density functional calculations · electronic structure · oligothiophenes · phospholes · pi-conjugation · Raman spectroscopy

Introduction

Thiophene is amongst the most commonly used aromatic building blocks for the tailoring of π-conjugated oligomers and polymers. Its high thermal and chemical stability and ease of functionalization are some of the reasons for its intensive use in this field.[1] In fact, the family of oligothiophenes (i.e., thiophene oligomers) is one of the most useful classes of organic conjugated systems. They have been successfully applied to a variety of optoelectronic devices such as light-emitting diodes (LEDs) and thin-film field-effect transistors (FETs).[1–4] Nonetheless, these homo-oligomers are not the best choice as far as band gap (i.e., HOMO–LUMO energy gap) is concerned. For instance, theoretical studies have revealed that the energy gaps of poly- and oligophospholes are considerably lower than those of their corresponding thiophene-based analogues.[5a,b] This is because phosphole is less aromatic than thiophene and hence its π system is more easily delocalized along a conjugated backbone. It is already well-established that the best properties of different building blocks can be maximized by preparing alternating mixed conjugated systems. With this in mind, the substitution of the central thiophene unit of terthiophene by phosphole has recently been carried out.[6] Furthermore, the reactivity of the phosphorus atom has been exploited to extend the family of these mixed phosphole–thiophene compounds.[6–8] These rather "simple" chemical modifications (i.e., oxidation, alkylation, etc.) permit fine-tuning of the physical properties of these compounds to yield novel materials for optoelectronics applications. This has been nicely illustrated by the report on thiophene-phosphole oligomers, the first organophosphorus conjugated material to be used for the fabrication of LEDs.[8]

After outlining the technological importance of these compounds, our purpose here is to shed further light on the mechanisms of electronic coupling in chains containing five-membered heterocycles of different aromaticity.[5,9] In particular, the insertion of phosphole within an oligothiophene has two significant advantages: 1) A decrease in the HOMO–LUMO gap[6a,d] and 2) the extra benefit of the versatile reactivity of the phosphorous atom allowing modification of its coordination number.[6–9] The reader will quickly realize that the principal electronic feature of all the trimers under study (Figure 1) is the competition between intra-ring delocalization (aromaticity) and inter-ring delocalization

[a] Dr. J. Casado, Prof. J. T. López Navarrete
Department of Physical Chemistry, University of Málaga
Campus de Teatinos s/n, Málaga 29071 (Spain)
Fax: (+34) 952-132-000
E-mail: teodomiro@uma.es

[b] Prof. R. Réau
Sciences Chimiques de Rennes
UMR 6226, CNRS-Université de Rennes 1, Campus de Beaulieu
35042 Rennes Cedex (France)

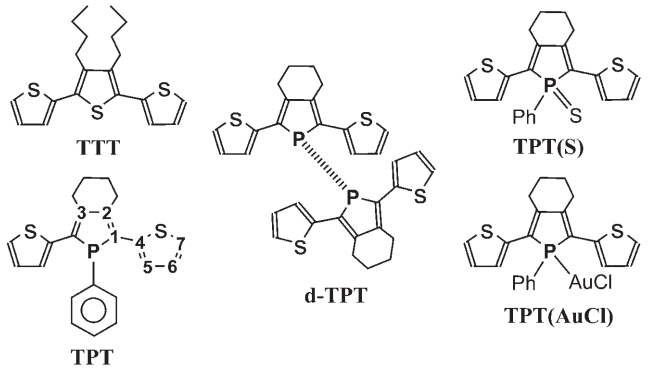

Figure 1. Chemical structures and abbreviations of the molecules studied in this work. The atom numbering in **TPT** is that used in Table 1.

(backbone π conjugation). The central focus of this paper is the study of the balance between these two types of delocalization as well as the modification through chemical functionalization of the phosphorus atom using Raman spectroscopy. Vibrational Raman spectroscopy will be employed as the main tool to monitor the electronic structure of the trimers under study, while quantum chemistry, UV/Vis absorption spectroscopy, and X-ray diffraction data will be used as auxiliary analytical methods. The suitability of Raman spectroscopy to the study of conjugational properties lies in the existence of a close relationship between the observed Raman lines and the π-conjugated structure.[10] Despite the high complexity of the Raman effect, it does provide intuitive ideas about this spectroscopic–structure relationship. The phenomenon originates in the existence of very effective electron–phonon coupling which results in some vibrational modes that mimic the evolution of the skeletal/electronic structure from the ground electronic state to the first accessible electronic state (S_1). In this class of polyconjugated molecules the dipole-allowed $S_0 \rightarrow S_1$ excitation is an electronic transition with a very high oscillator strength (vide infra) with which the molecule undergoes a very large reorganization of the electric dipole quantities and consequently of the molecular polarizabilities responsible for the Raman activity. As a result, those vibrations that couple both electronic states are expected to be very intense in the Raman spectrum.[10] It follows that the peak position of these enhanced Raman lines can be viewed as observables of the aromaticity/inter-ring conjugation electronic balance and that their wavenumbers can provide an estimation of the prevalence of one or the other.

This paper focuses on three 2,5-di(2-thienyl)phospholes [abbreviated as **TPT**, **TPT(S)**, and **TPT(AuCl)**] and the dimer **d-TPT** (Figure 1). The first family consists of "classical π-conjugated systems" in the sense that they feature an alternation of single and double bonds. **TPT(S)** and **TPT-(AuCl)** have been successfully used as materials for LEDs.[7] In **d-TPT**, through-bond or through-space interactions between the conjugated units can take place owing to the high polarizability and the low σ–σ* gap of the P–P bond, in analogy with the well-known Si–Si case.[8] The manuscript is structured in two main parts. First, the vibrational assignment of the main Raman lines based on the topologies of the normal modes obtained by theoretical calculations is presented; some intuitive relationships between structural parameters and Raman wavenumbers will be discussed. Second, once the nature of the Raman lines has been established, the Raman spectra upon thiophene/phosphole exchange (**TTT** versus **TPT**, Figure 1) and upon chemical modification of the phosphorus atom [**TPT(S)** and **TPT(AuCl)** versus **TPT**] will be interpreted.

Results and Discussion

Molecular structures and optical spectra of TPT and d-TPT: The most relevant experimental and calculated bond lengths for **TPT** and **d-TPT** are presented in Table 1 and Figure 2

Table 1. Experimental and calculated (B3LYP/6-31G**) geometric data for **TPT** and **d-TPT**.[a]

	TPT (exptl)	**TPT** (calcd)	**d-TPT** (exptl)	**d-TPT** (calcd)
P–C1	1.817(4)	1.831	1.802(5)	1.824
	1.818(5)		1.808(5)	
C1=C2	1.356(6)	1.375	1.360(6)	1.373
	1.366(6)		1.374(7)	
C2–C3	1.465(7)	1.470	1.459(7)	1.464
			1.454(6)	
C1–C4	1.446(6)[b]	1.446	1.459(7)	1.447
			1.462(6)	
C4–S	1.742(5)[b]	1.768	1.713(5)	1.764
			1.734(5)	
C4=C5	1.406(7)[b]	1.387	1.363(7)	1.386
			1.393(7)	
C5–C6	1.422(8)[b]	1.423	1.403(8)	1.424
			1.404(8)	

[a] Bond lengths are given in Å. For the atom numbering see Figure 1. [b] Values for the less disordered thienyl group.

shows two molecular views of the optimized structure of the P–P dimer species calculated at the B3LYP/6-31G** level of theory. Note that in the solid state, the thienyl rings of **TPT** exhibit a statistical disorder (*syn* and *anti* conformation with respect to the central phosphole ring), leading to some equalization of the thienyl bond lengths (Table 1).[6a] For **d-TPT**, theory predicts an all-*trans* conformation for the three five-membered rings and a pyramidal geometry for the two phosphorus atoms. The two **TPT** moieties are not slipped in between but displaced each other around the P–P bond (*gauche* conformation) probably due to the steric hindrance between the CH_2 groups. This optimized structure is in good agreement with the experimental X-ray diffraction study.[8] Very interestingly, on passing from **TPT** to **d-TPT**, theoretical and experimental data show subtle geometrical changes of the central phosphole ring (Table 1), while geometric data for the C=C/C–C bond lengths of the external thiophenes remain almost unaltered (Table 1).

The first focus of this analysis is the UV/Vis electronic absorption spectrum of **TPT** since 1) it is a prototype for this

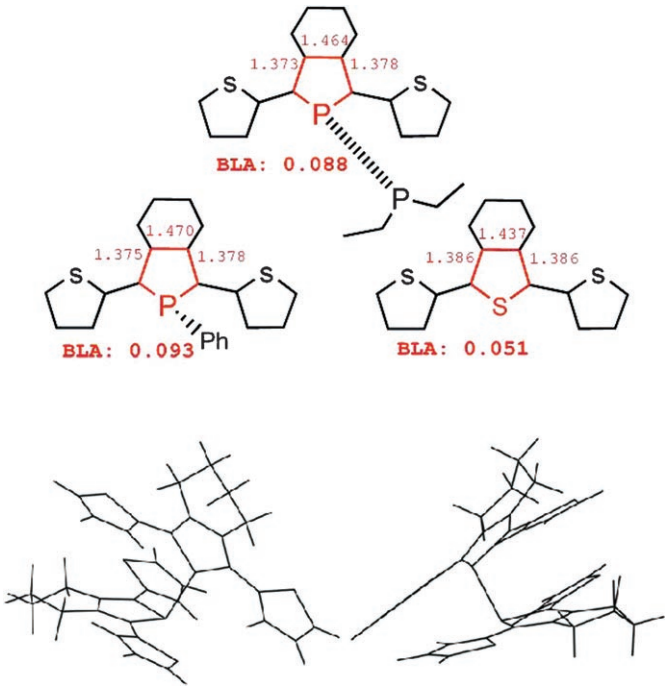

Figure 2. Molecular views of the optimized structure of **d-TPT** calculated at the B3LYP/6-31G** level of theory. Bond lengths and bond-length alternations (BLA) are given in Å.

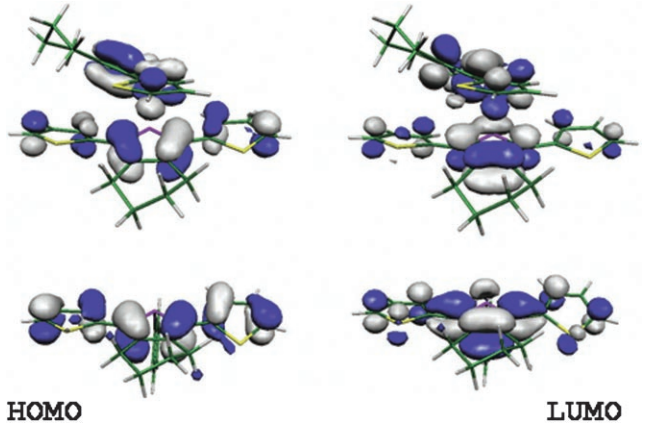

Figure 3. Orbital topologies of the HOMO and LUMO wavefunctions of **TPT** (bottom) and **d-TPT** (top).

series of phosphole-based compounds and 2) its theoretical simulation by time-dependent density functional theory leads to savings of computational costs (i.e., the lowest molecular weight). TD-DFT//B3LYP/6-31G** excited-state calculations predict that the lowest-lying $S_0 \rightarrow S_1$ electronic transition exhibits by far the largest oscillator strength within the 10 first electronic excitations of **TPT** which mostly occur in the UV/Vis spectral region.[11]

From these results, two important insights can be deduced. 1) The lowest-lying electronic band measured at 412 nm in **TPT** is related to the HOMO→LUMO ($S_0 \rightarrow S_1$) one-electron promotion calculated at 426 nm. 2) This excitation shows by far the largest oscillator strength and extinction coefficient for its associated absorption band in the Vis/NIR excitation spectrum which comprises the preresonance region of our Raman experiment ($\lambda_{exc} = 1064$ nm). The reader should bear in mind these two results throughout the paper since they support the principal arguments in the discussion on Raman intensity modulation and in the interpretation of the electron–phonon mechanism. To help with this discussion in the next sections, the topology of the components of this intense transition, the HOMO and LUMO orbitals of **TPT** and **d-TPT**, are shown in Figure 3.[8]

The HOMO–LUMO band of **TPT** is red-shifted by around 20 nm with respect to that of **TTT**, probably as a result of the higher ring aromaticity of thiophene relative to that of phosphole. Stronger aromatization stabilizes/destabilizes the HOMO/LUMO terms and enlarges their energy separation. Oxidation or coordination of phosphorus in **TPT(S)** and **TPT(AuCl)** fully disrupts the phosphole aromaticity, resulting in a destabilization/stabilization of the HOMO/LUMO energies and a concomitant displacement of the UV/Vis bands to lower energies by 30–40 nm.[6,7] The tuning of the wavelength maxima of the HOMO–LUMO band of the "nonaromatic" phosphorus-substituted derivatives must be related to electronic effects of different origins, probably sizable intramolecular charge transfer towards the central ring. In contrast, the HOMO–LUMO band in **d-TPT** appears at around 500 nm, a feature that must result from additional interactions, possibly electronic couplings between the two assembled **TPT** molecules mediated by the highly polarizable P–P bridge.[8] The next sections will try to shed light on these assumptions on the basis of data provided by Raman spectroscopy.

Experimental and theoretical Raman spectra: spectroscopic–structure correlations:

Assignment of the Raman spectra: Theory reproduces the vibrational Raman profiles of **d-TPT** quite well, as shown in Figure 4. On the other hand, Figure 5 depicts the vibrational eigenvectors associated with the most important lines of the experimental spectrum.

The Raman band at 1512 cm^{-1}, which is calculated to be at 1514 cm^{-1}, arises from an antisymmetric C=C stretching vibration of the outermost thiophene rings (see its eigenvector in Figure 5). Its homologous symmetric ν(C=C) thienyl stretching mode is associated with the experimental Raman line at 1416 cm^{-1} (1412 cm^{-1} in the theoretical spectrum). The highest energy band at 1555 cm^{-1} (calculated value, 1545 cm^{-1}) is due to an antisymmetric C=C stretching vibration of the phosphole rings. Its symmetric counterpart is associated with the strongest Raman line at 1465 cm^{-1}, predicted by B3LYP/6-31G** theory to be at 1456 cm^{-1}. Secondary Raman lines, like that measured at 1327 cm^{-1} (calculated value, 1305 cm^{-1}), can be described as a C–C stretching mode of the phosphole moiety while the thienyl homologue might be associated with the line at 1351 cm^{-1} (theoretically at 1337 cm^{-1}).

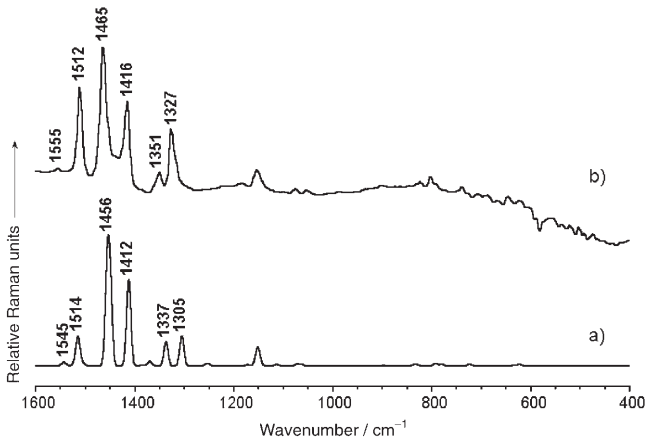

Figure 4. Comparison between a) the Raman spectrum of **d-TPT** calculated at the B3LYP/6-31G** level of theory and b) the experimental Raman spectrum.

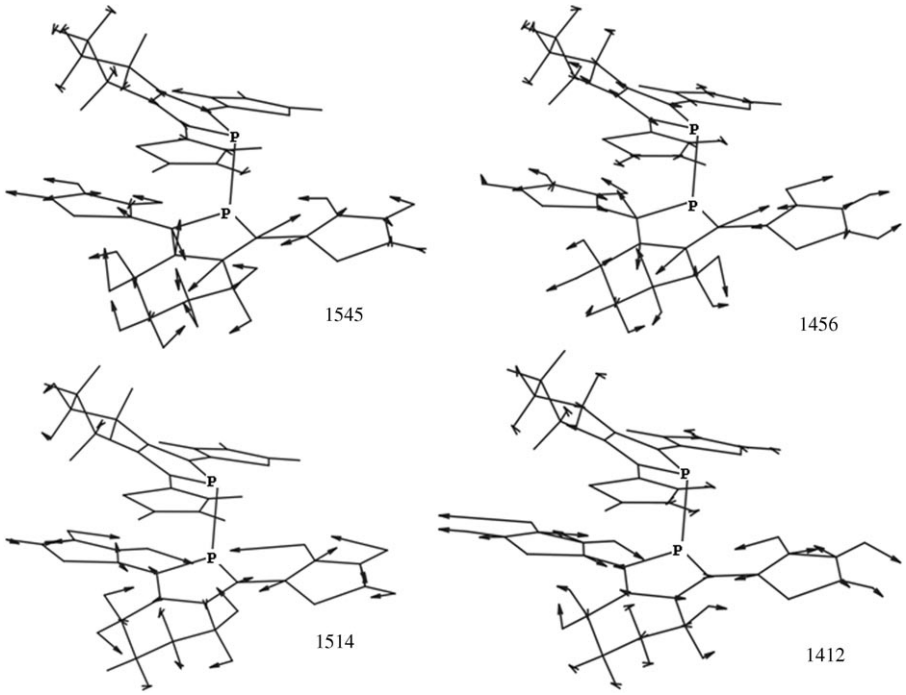

Figure 5. Vibrational eigenvectors associated with the most important lines of the theoretical spectrum of **d-TPT**. Theoretical values are given in cm^{-1}.

Electron–phonon coupling and Raman spectra: The experimental and theoretical geometries indicate that the skeletal/electronic structures of the co-oligomers are of heteroaromatic character (the side bonds of each five-membered ring have double-bond character while the CC bonds connecting them and the inter-ring bonds are single). Provided that the pure electronic contribution to the Raman activity comes from the lowest-lying electronic transition (HOMO→LUMO one-electron excitation), it is reasonable to assume that the quinoid profile described by the orbital topology of the LUMO (i.e., C=C/C−C bonding/antibonding interactions in S_0 become antibonding/bonding in S_1) makes a significant contribution to the structure of this first excited electronic-state. As a result, the normal modes effecting the largest changes in molecular polarizability and Raman intensity should correspond to vibrations that mimic the heteroaromatic→heteroquinoid ($S_0 \rightarrow S_1$) skeletal transition or C=C/C−C stretching vibrations. The Raman spectra of these trimers (vide infra) display only a few but very intense bands, all of them appearing in the C=C/C−C stretching region (1300–-1600 cm^{-1}). This feature reinforces the predictions of the extraordinary polarizability enhancement and selectivity that arise from the coupling of particular skeletal modes to the electronic structure or the electron–phonon mechanism.

On the relative Raman intensities of the C=C/C−C modes: From the previous analysis, it follows that 1) only the $S_0 \rightarrow S_1$ excitation is mainly involved in the preresonance region of our Raman experiment[12] and 2) this excitation consists of a one-electron HOMO→LUMO promotion implying an aromatic(S_0)→quinoid(S_1) evolution of the electronic structure. Consequently, the vibrational mode that better couples the molecular structures of these two states is that associated with the Raman mode at 1465 cm^{-1} (the phosphole C=C bond distances lengthen and the C−C bonds shorten) which is the strongest Raman line of the whole spectrum. On the other hand, the assignments made in the previous section show that the strongest Raman bands are divided into three sets of doublets wherein each component belongs to vibrational modes located either in the phosphole or in the thiophene subunits. For the highest wavenumber bands, the Raman lines associated with the stretching modes of the central phosphole are always the most intense. This distribution of the Raman intensities may be due to the fact that within the $S_0 \rightarrow S_1$ transition the largest reorganization of charge density, the greatest contribution to the oscillator strength and to the polarizability moment transition (Raman activity),[12] occurs in the central phosphole, thus explaining the high intensity of its antisymmetric and symmetric C=C/C−C stretches. Hence, the corresponding thienyl vibrations are secondary bands as these peripheral groups are less involved in the dominant electronic transition.

Raman wavenumbers and molecular structure: Let us now focus our attention on the ring character of these vibrations and the intimate relationship between their wavenumbers

and some ring structural parameters. The C=C bond lengths calculated at the B3LYP/6-31G** level of theory are very similar for thiophene (1.371 and 1.386 Å) and phosphole (1.375 and 1.378 Å). It is thus not clear which C=C stretching would appear at a higher or lower wavenumber. The bond-length alternation (BLA) is a structural parameter equivalent to the Julg index and, like the nucleus-independent chemical shift (NICS) magnetic criteria, is a reliable approach to the evaluation of ring aromaticity.[13] The BLA is the average of the differences between consecutive CC bonds of a given C=C/C−C path. To some extent, this parameter is a measure of the phenomenon of bond-length equalization, which is a characteristic of aromatic rings (i.e., BLA for benzene is 0 and 0.063 Å for thiophene according to B3LYP/6-31G** calculations). Deviations from these values might be interpreted as a disruption of ring aromaticity in favor of inter-ring C=C/C−C conjugation in the case of our α,α′ linearly connected five-membered rings.

Assuming the relationship between these criteria and their reliability to account for aromaticity (even the concept itself is questionable), we have tried to correlate ring BLA data and Raman wavenumbers. It is not our intention to establish new spectroscopic methods for measuring ring aromaticity, but the realization of spectroscopic and structural quantities that likely share a common origin. The general validity of this finding should require much more extensive analyses and structure/spectroscopic elucidations (beyond the scope of the present study). In this regard, the reader is referred to a recent publication that shows quite relevant Raman-wavenumber/BLA relations and their dependence on the nature of the substitution in aromatic oligothiophenes.[14]

The computed BLA values for the thiophene and phosphole rings of **d-TPT** are, respectively, 0.0485 and 0.0885 Å (Figure 2), reflecting a great degree of ring CC bond-length equalization in the thienyl moieties. This feature is in accord with the greater aromatic character of thiophene relative to phosphole. In contrast to the consideration of individual bonds lengths, a correlation exists between ring BLA and Raman peak positions in the sense that the lower wavenumbers of the thienyl bands agree with the lower BLA value for thiophene, somehow revealing the connection between ring structure and ring vibrations. On the other hand, this result evidences the segmentation of the electronic structure of **d-TPT** as well as that of its monomer homologue **TPT**, as will be shown by comparison with terthiophene (**TTT**). In the next section we focus on the electronic properties after phosphole functionalization and it will be shown that the above-described spectroscopic/structure correlation still holds upon chemical complexation or oxidation of the phosphorus of the phosphole center.

Raman spectra upon chemical functionalization:

*Comparison of **TTT** and **TPT***: Figure 6 depicts the FT-Raman spectra of **TTT**, **TPT**, and its **TPT(AuCl)** and **TPT(S)** derivatives.

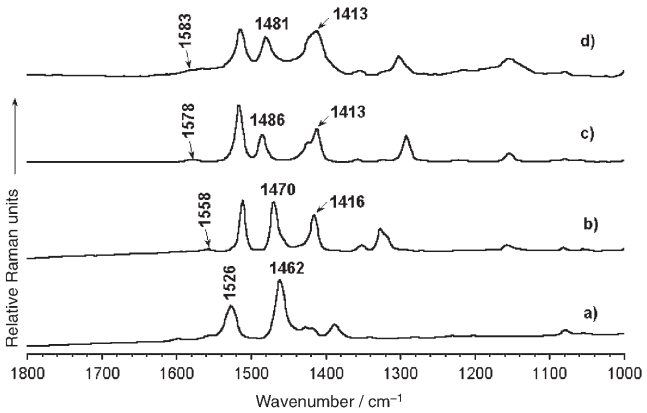

Figure 6. FT-Raman spectra of a) **TTT**, b) **TPT**, c) **TPT(S)**, and d) **TPT-(AuCl)**.

Two important lines at 1526 and 1462 cm^{-1} are observed in the spectrum of **TTT** which correspond to the antisymmetric and symmetric C=C stretching modes mainly located in the external and internal rings, respectively.[15] For our purposes, the peak position of the central-ring vibration at 1462 cm^{-1} of **TTT** can be compared with the wavenumbers of the phosphole-ring vibrations of the mixed co-oligomers. The wavenumbers of these stretches (**TPT**, 1470 cm^{-1}; **TTT**, 1462 cm^{-1}) are in agreement with the lowering of the BLA of the central ring on passing from **TPT** (0.093 Å) to **TTT** (0.051 Å). This is also in accordance with the greater aromaticity of thiophene relative to phosphole. The very low aromatic character of phosphole is well documented to be caused by the nonplanar conformation of the phosphorus and the high s character of its lone electron pair, two factors which prevent efficient delocalization of the sextet over the ring.[9d–f] In fact the whole effect of phosphorus aromatization within the phosphole ring (i.e., the interaction of the P−R fragment with the *cis*-butadiene moiety) can be divided into two contributions: 1) The interaction between the π* vacant orbitals of butadiene and the lone electron pair orbital of the phosphorus atom and 2) the hyperconjugative interaction between the π-occupied orbitals of the butadiene group and the exocyclic P−C bond (the energy of this bond is in the range of the π bonds).[9e,i] Halfway between these two effects, the presence of bulky substituents connected to the phosphorus atom facilitates its planarization thus increasing phosphole aromaticity (vide infra).[9d–f]

***TPT** upon functionalization: The phenomenon of ICT*: This section is concerned with the first case, that is, the interaction between the butadiene moiety and the phosphorus atom and is exemplified by means of the analysis of the Raman spectra upon functionalization of **TPT** through the phosphorus lone electron pair. The most noticeable feature is the upshift of the band associated with the phosphole ν_s-(C=C) mode which moves from 1470 cm^{-1} in **TPT** to 1481 cm^{-1} in **TPT(AuCl)** and to 1486 cm^{-1} in **TPT(S)** (Figure 6).

Oxidized or coordinated phosphole rings are clearly not 6π electron systems. As a consequence, the double bonds of the central five-membered ring are strengthened and the single bond weakened (namely, the B3LYP/6-31G** calculated central-ring C=C/C–C bond lengths change from 1.375/1.470 Å in **TPT** to 1.370/1.486 Å in **TPT(S)**) resulting in a decrease in bond equalization (increase of BLA) and a shift of the Raman lines associated with ring stretches to higher energies. In addition to the reduction in phosphole aromaticity, accompanied by the upshift of the Raman bands, other phenomena must exist to account for the different appearance of the Raman peaks in **TPT(AuCl)** and **TPT(S)**. The central phosphorus five-membered heterocycle becomes a partially electron-deficient center upon oxidation/complexation and a certain degree of intramolecular charge transfer (ICT) from the outer electron-rich thiophenes to the central electron-withdrawing ring might be expected. This ICT results in a partial quinoidization of the structure, as shown in Scheme 1 (i.e., a weakening of the

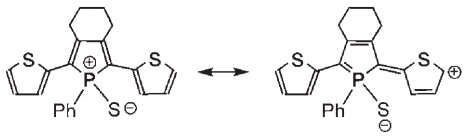

Scheme 1. Quinoidization of **TPT(S)** due to ICT.

double bonds and a strengthening of the single ones), and is supported by the wavenumber downshift of the ν(C=C) ring stretching vibrations (i.e., 1486 cm^{-1} in **TPT(S)** and 1481 cm^{-1} in **TPT(AuCl)**). This phenomenon takes place upon tetra-/penta-coordination of the phosphorus atom and, therefore, is more marked in the central ring than in the outer thiophenes. Moreover, the impact on these external rings is further attenuated by the fact that the whole effect is shared by two thiophenes and, hence, a small downshift of the ν_a(C=C) thienyl Raman wavenumbers is observed from 1517 cm^{-1} in **TPT(AuCl)** to 1515 cm^{-1} in **TPT(S)** (see Figure 6). ICT might influence the atomic charge distribution as well, hence the charges on the outer thiophene rings, although very subtly for the above reasons, evolve as $-0.043e \rightarrow -0.040e$ on **TPT**→**TPT(S)**, while the positive charge on the central phosphorus ring is significantly neutralized upon oxidation of the phosphorus atom with sulfur ($+0.304e$ in **TPT** and $+0.001e$ in **TPT(S)**). One more detail that might confirm the charge redistribution upon ICT is the large charge density ($-0.361e$) located on the central sulfur atom of **TPT(S)** (Scheme 1).

*Comparison of **TPT** and **d-TPT**: Through-bond interactions*: In contrast to the above wavenumber-upshift noticed upon oxidation/complexation of the phosphorus atom, the ν(C=C) Raman lines of **d-TPT** are displaced to lower energies with respect to **TPT** while the thienyl bands remain unaltered (Figure 7). These observations should reflect the phenomenon of hyperconjugation between the butadiene group and

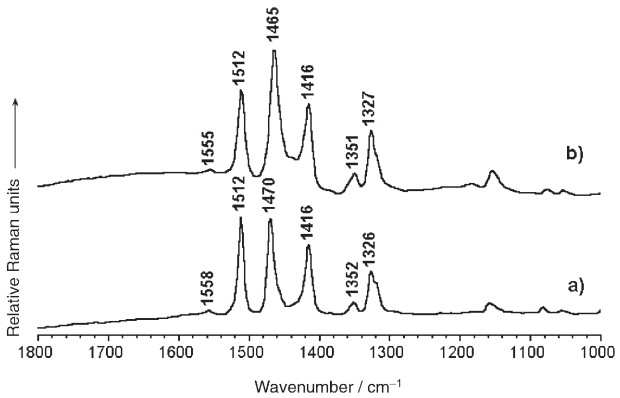

Figure 7. Solid-state FT-Raman spectra of a) **TPT** and b) **d-TPT**.

the exocyclic P–C bond mentioned above. This phenomenon is observed spectroscopically in the dimer through the 3 and 5 cm^{-1} downshift of the ν(C=C) phosphole stretches, which is in agreement with a slight decrease in the BLA on going from **TPT** (0.093 Å) to **d-TPT** (0.088 Å), an evolution that is consistent with a slight bond-length equalization or increased phosphole aromaticity in **d-TPT**. On the other hand, negligible BLA changes have been predicted for the outermost thiophene rings in agreement with the constant peak position of their associated Raman lines. Note at this point that the theoretical data derived from DFT theory should be regarded with some caution as a result of its intrinsic limitations. However their good correlation with experiments must be stressed despite the inherent difficulty (very small spectroscopic changes) associated with the subtle effects taking place in the electronic structures of these systems. In this sense, it is interesting to highlight how the calculations and spectroscopic data pretty well agree in the evaluation of ring structural parameters.

Upon formation of a P–P bond, a favored scenario for phosphole ring aromaticity is expected. Upon substitution of the phosphorus atom with a bulkier group **(Ph**→**TPT)**, it is possible to argue that a flattening of the phosphole ring might facilitate ring aromaticity. However, this hypothesis has to be ruled out since the so-called "pyramidality" of the tri-coordinate phosphorus atom (given by the sum of the CPX angles obtained by X-ray diffraction study) is 310.4° in **TPT** and 311.4° in **d-TPT**, showing that the phosphorus atoms have very similar geometries.

The spectroscopic downshift of the ν(C=C) phosphole stretches in the assembled molecule may also be rationalized in terms of the hyperconjugation between the π(butadiene) and the P–C/P–P bonds. This phenomenon is favored in the presence of a more polarizable P–P bond (i.e., a higher energy of the σ term of the P–P bond in **d-TPT** with regard its P-C parent). This mechanism likely induces a slight increase in the aromaticity of the phosphole ring in the dimer system, accompanied by certain bond-length equalization and a red shift of the stretching Raman modes. This description represents a through-bond interaction between the two π chromophores that leads to electronic cou-

pling of their frontier orbitals. This feature is probably the origin of the reduction of the HOMO–LUMO energy gap relative to the P–Ph molecules (HOMO–LUMO band: **d-TPT**, 500 nm; **TPT**, 412 nm, vide supra).

Raman spectra in solution and thermospectroscopic study: To gain more insight into the nature of the coupling of the two **TPT** components in the dimer, the Raman spectrum of **d-TPT** was recorded in dichloromethane (Figure 8). Comparison between the solid-state and solution Raman spectra shows that the phosphole ν_s(C=C) line is upshifted by 4 cm^{-1} (1469 cm^{-1}), whereas the thiophene ν_a(C=C) line scarcely changes.

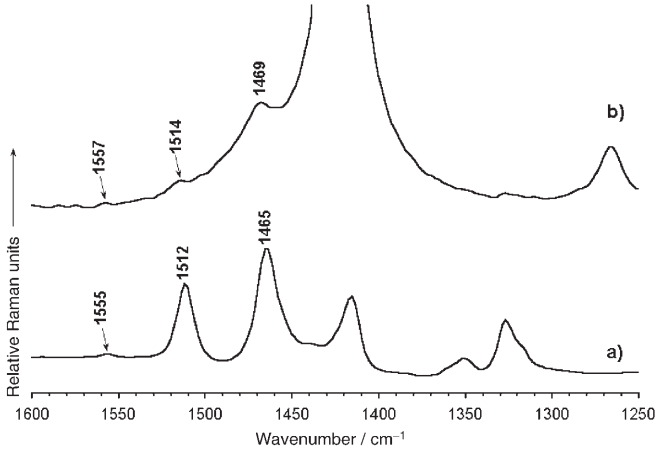

Figure 8. FT-Raman spectra of a) **d-TPT** in the solid state and b) **d-TPT** in dichloromethane.

To further investigate the solid-state interactions, the evolution of the Raman spectrum of **d-TPT** was analyzed as a function of temperature. By cooling the solid material, the phosphole and thiophene ν_s(C=C) wavenumbers are shifted to slightly higher values (phosphole, 1465 cm^{-1} (100 °C)→ 1467 cm^{-1} (−170 °C); thiophene, 1512 cm^{-1} (100 °C)→ 1513 cm^{-1} (−170 °C)). At low temperatures, the intermolecular and through-space interactions between the two **TPT** chromophores are expected to be particularly promoted while through-P–P-bond interactions should in principle coalesce. The minimal thermospectroscopic changes seem to dismiss the involvement of significant through-space π–π* interactions in **d-TPT**. Moreover, the evolution of the spectra with varying temperature and in solution is likely induced by local weak interactions affecting the phosphorus atoms (i.e., solvation, solvent–solute interactions or hydrogen bonds with neighboring hydrogen atoms in the solid state). Overall, these results reinforce the hypothesis that through-bond interactions between the two chromophores in the P–P dimer are the relevant electronic effect in this assembled system.

Conclusion

In this paper the electronic structure of a very new class of molecules that combines thiophene and phosphole units has been explored with special emphasis on their π-electron conjugational properties. The study is principally concerned with Raman spectroscopy but is partially guided by theoretical calculations (DFT//B3LYP/6-31G** methodology) and UV/Vis absorption spectroscopy. This work highlights the use of vibrational Raman spectroscopy as an incisive probe of the structure of this class of conjugated systems and serves to outline significant structure–property relationships. Two differentiated groups of bands exist that belong to either the central phosphole or the outer thiophene. This band division reveals a certain degree of segmentation of the structure which is particularly interesting with regard the promotion of the electronic interactions needed to improve the optical properties of phosphole-based π-conjugated systems.

A correlation between the wavenumber of the strongest Raman lines and the BLA structural parameter has been proposed to evaluate the modulation of the electronic properties. In this regard, the changes in the Raman band wavenumbers have been successfully discussed in terms of 1) thiophene/phosphole aromaticity (ring bond-length equalization), 2) the oxidation or complexation of phosphorus, followed by intramolecular charge transfer and sizable structural quinoidization, and 3) the hyperconjugation of the exocyclic P–P bond in thienyl-capped 1,1′-diphosphole which promotes better phosphole aromatization. In conclusion, this work rationalizes how electronic properties in conjugated thienyl-phosphole co-oligomers are particularly balanced by subtle aromatic/conjugating interactions and illustrates how an efficient spectroscopic method (Raman spectroscopy) may be used to monitor important structural and electronic parameters that play an essential role in the design of new organo-phosphorus materials.[16]

Experimental and Theoretical Details

Details of the synthetic procedures and characterization of the molecules depicted in Figure 1 have already been reported elsewhere.[6–8] FT-Raman spectra were recorded by using an FT-Raman accessory kit (FRA/106-S) of a Bruker Equinox 55 FT-IR interferometer. A continuous wave of a Nd:YAG laser operating at 1064 nm was employed for excitation. A germanium detector operating at liquid-nitrogen temperature was used. Raman scattering radiation was collected in a back-scattering configuration using a standard spectral resolution of 4 cm^{-1}. The power of the laser radiation was always kept lower than 100 mW and 1000–3000 scans were averaged for each spectrum.

A variable-temperature Specac P/N 21525 cell with interchangeable pairs of quartz windows was used to record the FT-Raman spectra at different temperatures. The variable-temperature cell consists of a surrounding vacuum jacket (0.5 Torr) and combines a refrigerant Dewar and a heating block as the sample holder. It was also equipped with a copper–constantan thermocouple for temperature monitoring purposes and any temperature, from −170 to 150 °C, could be achieved. Samples were inserted into the heating block or the Dewar/cell holder assembly as pure solids in a quartz cell and Raman spectra were recorded after waiting for the

sample to reach thermal equilibrium, which required 20 min for every increment of 10 °C.

Density functional theory (DFT) calculations were carried out using the Gaussian 98 program on an SGI Origin 2000 supercomputer.[17] We used Becke's three-parameter exchange functional combined with the LYP correlation functional (B3LYP).[18] It has already been shown that the B3LYP functional yields similar geometries for medium-sized molecules as MP2 calculations do with the same basis sets.[19] Moreover, the DFT force fields calculated using the B3LYP functional yield vibrational spectra in very good agreement with experiments.[20] We also made use of the standard 6-31G** basis set.[21] Optimal geometries were determined on isolated entities. All geometrical parameters were allowed to vary independently. Vertical electronic excitation energies were computed by using the time-dependent DFT (TDDFT) approach.[22,23] For the resulting ground-state optimized geometries, harmonic vibrational frequencies, and Raman intensities were calculated numerically using the B3LYP functional. Calculated harmonic vibrational frequencies were uniformly scaled down by a factor of 0.96 as recommended by Scott and Radom for the 6-31G** basis set.[20a] All quoted theoretical vibrational frequencies reported are thus scaled values.

Acknowledgements

J.C. is grateful to the Ministerio de Educación y Ciencia (MEC) of Spain for a Ramón y Cajal research position at the University of Málaga. The present work was supported in part by the Dirección General de Enseñanza Superior (DGES, MEC, Spain) through the research project BQU2003-03194. We are also indebted to the Junta de Andalucía (Spain) for funding our research group (FQM-0159). R.R. thanks the Ministère de l'Education Nationale de la Recherche et la Technologie, the Institut Universitaire de France and the Centre National de la Recherche Scientifique.

[1] a) K. Müllen, G. Wegner, *Electronic Materials: The Oligomer Approach*, Wiley-VCH, Weinheim, **1998**; b) J. Roncali, *Chem. Rev.* **1997**, *97*, 173; c) J. M. Tour, *Acc. Chem. Res.* **2000**, *33*, 791; d) E. A. Meyer, R. K. Castellano, F. Diederich, *Angew. Chem.* **2003**, *115*, 1244; *Angew. Chem. Int. Ed.* **2003**, *42*, 1210; e) T. A. Skotheim, R. L. Elsenbaumer, J. R. Reynolds, *Handbook of conducting polymers*, 2nd ed., Marcel Dekker, New York, **1998**; f) H. S. Nalwa, *Handbook of conductive materials and polymers*, Wiley, New York, **1997**.

[2] H. Akimichi, K. Waragai, S. Hotta, H. Kano, H. Sakaki, *Appl. Phys. Lett.* **1991**, *58*, 1500; F. Garnier, A. Yassar, R. Hajlaoui, G. Horowitz, D. Deloffre, B. Servet, S. Ries, P. Alnot, *J. Am. Chem. Soc.* **1993**, *115*, 8716.

[3] C. D. Dimitrakopoulos, P. R. L. Malenfant, *Adv. Mater.* **2002**, *14*, 99; H. E. Katz, Z. Bao, S. L. Gilat, *Acc. Chem. Res.* **2001**, *34*, 359.

[4] A. Facchetti, Y. Deng, A. Wang, Y. Koide, H. Sirringhaus, T. J. Marks, R. H. Friend, *Angew. Chem.* **2000**, *112*, 4721; *Angew. Chem. Int. Ed.* **2000**, *39*, 4547; A. Facchetti, M. Mushrush, H. E. Katz, T. J. Marks, *Adv. Mater.* **2003**, *15*, 33; A. Facchetti, M.-H. Yoon, C. L. Stern, H. E. Katz, T. J. Marks, *Angew. Chem.* **2003**, *115*, 4030; *Angew. Chem. Int. Ed.* **2003**, *42*, 3900; T. M. Pappenfus, R. J. Chesterfield, C. D. Frisbie, J. Casado, J. D. Raff, L. L. Miller, K. R. Mann, *J. Am. Chem. Soc.* **2002**, *124*, 4184.

[5] a) U. Salzner, J. B. Lagowski, P. G. Pickup, R. A. Poirier, *Synth. Met.* **1998**, *96*, 177; b) J. Ma, S. Li, Y. Jiang, *Macromolecules* **2002**, *35*, 1109; c) M. Hissler, P. Dyer, R. Réau, *Coord. Chem. Rev.* **2003**, *244*, 1; d) D. Delaere, A. Dransfeld, M. T. Nguyen, L. G. Vanquickenborne, *J. Org. Chem.* **2000**, *65*, 2631; e) D. Delaere, M. T. Nguyen, L. G. Vanquickenborne, *Phys. Chem. Chem. Phys.* **2002**, *4*, 1522.

[6] a) C. Hay, M. Hissler, C. Fischmeister, J. Rault-Berthelot, L. Toupet, L. Nyulászi, R. Réau, *Chem. Eur. J.* **2001**, *7*, 4222; b) C. Hay, D. Le Vilain, V. Deborde, L. Toupet, R. Réau, *Chem. Commun.* **1999**, 345; c) C. Hay, C. Fischmeister, M. Hissler, L. Toupet, R. Réau, *Angew. Chem.* **2000**, *112*, 1882; *Angew. Chem. Int. Ed.* **2000**, *39*, 1812; d) C. Hay, C. Fave, M. Hissler, J. Rault-Berthelot, R. Réau, *Org. Lett.* **2003**, *5*, 3467; e) C. Fave, M. Hissler, K. Sénéchal, I. Ledoux, J. Zyss, R. Réau, *Chem. Commun.* **2002**, 1674; f) M. Hissler, P. W. Dyer, R. Réau, *Topics in Current Chemistry: New Aspects in Phosphorus Chemistry V* (Ed.: J. P. Majoral), Springer, Heidelberg, **2005**.

[7] a) C. Fave, T. Y. Cho, M. Hissler, C. W. Chen, T. Y. Luh, C. C. Wu, R. Réau, *J. Am. Chem. Soc.* **2003**, *125*, 9254; b) H.-C. Su, O. Fadhel, C.-J. Yang, T.-Y. Cho, C. Fave, M. Hissler, C.-C. Wu, R. Réau, *J. Am. Chem. Soc.* **2006**, *128*, 983.

[8] C. Fave, M. Hissler, T. Kárpáti, J. Rault-Berthelot, V. Deborde, L. Toupet, L. Nyulászi, R. Réau, *J. Am. Chem. Soc.* **2004**, *126*, 6058.

[9] For other types of thiophene-phosphole derivatives, see: a) M.-O. Bevière, F. Mercier, L. Ricard, F. Mathey, *Angew. Chem.* **1990**, *102*, 672; *Angew. Chem. Int. Ed. Engl.* **1990**, *29*, 655; b) M.-O. Bévierre, F. Mercier, F. Mathey, A. Jutand, C. Amatore, *New J. Chem.* **1991**, *15*, 545; c) T. Baumgartner, T. Neumann, B. Wirges, *Angew. Chem.* **2004**, *116*; *Angew. Chem. Int. Ed.* **2004**, *43*, 6197; d) L. Nyulaszi, *Chem. Rev.* **2001**, *101*, 1229; e) W. Schaefer, A. Schweig, F. Mathey, *J. Am. Chem. Soc.* **1976**, *98*, 407; f) *Phosphorus: the Carbon Copy* (Eds.: K. B. Dillon, F. Mathey, J. F. Nixon), John Wiley and Sons, Chichester, **1998**; g) *Phosphorus-carbon Heterocyclic Chemistry: the rise of a New Domain* (Ed.: F. Mathey), Pergamon Press, Oxford, **2001**; h) E. Mattmann, F. Mathey, A. Sevin, G. Frison, *J. Org. Chem.* **2002**, *67*, 1208; i) W. Schäfer, A. Schweig, F. Mathey, *J. Am. Chem. Soc.* **1976**, *98*, 407; j) T. Baumgartner, W. Bergmans, T. Karpati, T. Neumann, M. Nieger, L. Nuyalaszi, *Chem. Eur. J.* **2005**, *11*, 4687.

[10] a) G. Zerbi, C. Castiglioni, M. Del Zoppo, *Electronic Materials: The Oligomer Approach*, Wiley-VCH, Weinheim, **1998**, p. 345; b) M. Gusoni, C. Castiglioni, G. Zerbi, *Spectroscopy of Advanced Materials*, Wiley, New York, **1991**, p. 251; c) C. Castiglioni, M. Del Zoppo, G. Zerbi, *J. Raman Spectrosc.* **1993**, *24*, 485; d) B. Horovitz, *Phys. Rev. Lett.* **1981**, *47*, 1491.

[11] The following quantities (transition: wavelength, oscillator strength, one-electron descriptions) are predicted at the B3LYP/6-31G** level of theory for the first 10 states: $S_0 \rightarrow S_1$: 426 nm, $f = 0.73$, HOMO $\rightarrow$ LUMO; $S_0 \rightarrow S_2$: 341 nm, $f = 0.002$, HOMO $\rightarrow$ LUMO+1; $S_0 \rightarrow S_3$: 320 nm, $f = 0.005$, HOMO-2 $\rightarrow$ LUMO; $S_0 \rightarrow S_4$: 313 nm, $f = 0.013$, HOMO-2 $\rightarrow$ LUMO and HOMO $\rightarrow$ LUMO+2; $S_0 \rightarrow S_5$: 296 nm, $f = 0.015$, HOMO $\rightarrow$ LUMO+3; $S_0 \rightarrow S_6$: 286 nm, $f = 0.013$, HOMO-5 $\rightarrow$ LUMO and HOMO-3 $\rightarrow$ LUMO; $S_0 \rightarrow S_7$: 279 nm, $f = 0.004$, HOMO-4 $\rightarrow$ LUMO and HOMO $\rightarrow$ LUMO+4; $S_0 \rightarrow S_8$: 277 nm, $f = 0.012$, HOMO-4 $\rightarrow$ LUMO, HOMO-5 $\rightarrow$ LUMO and HOMO-3 $\rightarrow$ LUMO; $S_0 \rightarrow S_9$: 273 nm, $f = 0.0006$, HOMO-6 $\rightarrow$ LUMO; $S_0 \rightarrow S_{10}$: 271 nm, $f = 0.082$, HOMO $\rightarrow$ LUMO+2, HOMO-2 $\rightarrow$ LUMO and HOMO-1 $\rightarrow$ LUMO.

[12] This picture of the Raman experiment is also based on the two-state model of Peticolas, see for example: W. L. Peticolas, D. P. Strommen, V. Lakshminarayanan, *J. Chem. Phys.* **1980**, *73*, 4185.

[13] A. Julg, P. Francois, *Theor. Chim. Acta* **1967**, *7*, 249; P. von R. Scheleyer, C. Maerker, A. Dransfeld, H. Jiao, N. J. R. E. Hommes, *J. Am. Chem. Soc.* **1996**, *118*, 6317; F. De Proft, P. Geerlings, *Chem. Rev.* **2001**, *101*, 1451; J. L. Brédas, *J. Chem. Phys.* **1985**, *82*, 3808.

[14] J. Casado, V. Hernández, R. Ponce Ortiz, M. C. Ruiz Delgado, J. T. López Navarrete, A. Facchetti, T. J. Marks, *J. Am. Chem. Soc.* **2005**, *127*, 13364.

[15] J. Casado, T. M. Pappenfus, L. L. Miller, K. R. Mann, E. Ortí, P. M. Viruela, R. Pou-Amerigo, V. Hernández, J. T. López Navarrete, *J. Am. Chem. Soc.* **2003**, *125*, 2534; J. Casado, V. Hernández, O.-K. Kim, J. M. Lehn, J. T. López Navarrete, S. Delgado Ledesma, R. Ponce Ortiz, M. C. Ruiz Delgado, Y. Vida, E. Pérez Inestrosa, *Chem. Eur. J.* **2004**, *10*, 3805; R. Ponce Ortiz, M. C. Ruiz Delgado, J. Casado, V. Hernández, O.-K. Kim, H. Y. Woo, J. T. López Navarrete, *J. Am. Chem. Soc.* **2004**, *126*, 13363.

[16] a) S. S. H. Mao, T. Don Tilley, *Macromolecules* **1997**, *30*, 5566; b) Y. Morisaki, Y. Aiki, Y. Chujo *Macromolecules* **2003**, *36*, 2594; c) R. C. Smith, J. D. Protasiewicz, *J. Am. Chem. Soc.* **2004**, *126*, 2268; d) V. A. Wright, D. P. Gates, *Angew. Chem.* **2002**, *114*; *Angew.*

Chem. Int. Ed. **2002**, *41*, 866; e) R. C. Smith, X. Chen, J. D. Protasiewicz, *Inorg. Chem.* **2003**, *42*, 5468; f) M. Hissler, P. W. Dyer, R. Réau, *Top. Curr. Chem.* **2005**, *250*, 127.

[17] Gaussian 98, Revision A.7, M. J. Frisch, G. W. Trucks, H. B. Schlegel, G. E. Scuseria, M. A. Robb, J. R. Cheeseman, V. G. Zakrzewski, J. A. Montgomery, R. E. Stratman, S. Burant, J. M. Dapprich, J. M. Millam, A. D. Daniels, K. N. Kudin, M. C. Strain, O. Farkas, J. Tomasi, V. Barone, M. Cossi, R. Cammi, B. Mennucci, C. Pomelli, C. Adamo, S. Clifford, G. Ochterski, A. Petersson, P. Y. Ayala, Q. Cui, K. Morokuma, D. K. Malick, A. D. Rabuck, K. Raghavachari, J. B. Foresman, J. Cioslowski, J. V. Ortiz, B. B. Stefanov, G. Liu, A. Liashenko, I. Piskorz, I. Komaromi, R. Gomperts, R. L. Martin, D. J. Fox, T. Keith, M. A. Al-Laham, C. Y. Peng, A. Manayakkara, C. Gonzalez, M. Challacombe, P. M. W. Gill, B. G. Johnson, W. Chen, M. W. Wong, J. L. Andres, M. Head-Gordon, E. S. Replogle, J. A. Pople, Gaussian Inc., Pittsburgh, **1998**.

[18] A. D. Becke, *J. Chem. Phys.* **1993**, *98*, 1372.

[19] J. J. Novoa, C. Sosa, *J. Phys. Chem.* **1995**, *99*, 15837; P. J. Stephens, F. J. Devlin, F. C. F. Chabalowski, M. J. Frisch, *J. Phys. Chem.* **1994**, *98*, 11623.

[20] A. P. Scott, L. Radom, *J. Phys. Chem.* **1996**, *100*, 16502; G. Rauhut, P. Pulay, *J. Phys. Chem.* **1995**, *99*, 3093.

[21] M. M. Francl, W. J. Pietro, W. J. Hehre, J. S. Binkley, M. S. Gordon, D. J. Defrees, J. A. Pople, *J. Chem. Phys.* **1982**, *77*, 3654.

[22] E. Runge, E. K. U. Gross, *Phys. Rev. Lett.* **1984**, *52*, 997; E. K. U. Gross, W. Kohn, *Adv. Quantum Chem.* **1990**, *21*, 255.

[23] Vertical electronic excitation energies and oscillator strengths were computed by using the TD-DFT approach. At least the 30 lowest-energy electronic excited-states were computed. TD-DFT calculations were carried out at the B3LYP/6-31G** level of theory.

Received: September 20, 2005
Published online: March 7, 2006

